Food Research International 239 (2026) 119614

Contents lists available at ScienceDirect

Food Research International

journal homepage: www.elsevier.com/locate/foodres

Unravelling the multi-scale structural organisation of *in vivo* ileal digesta from diets containing protein–seaweed polysaccharide blends

Yubexi Correa [a], Natalia S. Fanelli [b], Juan Carlos Martínez [c], Cristina Jiménez-Holgado [a], Isidra Recio [a], Hans H. Stein [b], Marta Martínez-Sanz [a,*]

[a] Instituto de Investigación en Ciencias de la Alimentación, CIAL (CSIC-UAM, CEI UAM + CSIC), Nicolás Cabrera, 9, 28049 Madrid, Spain
[b] Department of Animal Sciences, University of Illinois at Urbana-Champaign, Urbana, IL 61801, USA
[c] ALBA Synchrotron Light Facility, Carrer de la Llum 2-26, 08290, Cerdanyola del Vallès, Barcelona, Spain

ARTICLE INFO

Keywords:
Gastrointestinal digestion
Dietary fibres
Protein-polysaccharide interactions
Bile salts
Ileal digesta
Small-angle X-ray scattering
Animal model

ABSTRACT

Seaweed-derived polysaccharides such as agar, alginate, carrageenan, and cellulose are increasingly used as functional ingredients in food products, yet their influence on the gastrointestinal digestion process remains poorly understood. This study investigated how different fibres modulate the digestion and nanoassembly process of two model food proteins, casein and whey protein isolate, under physiologically relevant conditions using an *in vivo* pig model. Ileal digesta were analysed through compositional, rheological, microstructural, and nanostructural characterisation. The results demonstrated that the proteins were extensively hydrolysed and largely absorbed before reaching the ileum in all the formulations. However, some peptidic fragments were particularly resistant to digestion when agar was added to WPI. The seaweed polysaccharides were not digested and showed different types of structures, with alginate generating dense network-like structures, while carrageenan and agar generated more homogeneous digesta. Cellulose was associated with the presence of more ordered nanomicellar structures, likely involving bile salts. This behaviour suggests alterations in bile salt organisation and availability, potentially related to changes in diffusion, retention or reabsorption. These findings suggest that seaweed polysaccharides do not impair protein digestibility, but they affect the micro- and nanostructural organisation of ileal digesta, primarily by modulating viscosity and colloidal assembly. Therefore, it is highly relevant to understand the impact of dietary fibres on the intestinal transport of nutrients, providing the basis for designing functional foods with improved nutritional quality.

1. Introduction

The need for sustainable and nutrient-dense food sources increases as the world's population grows. Alternative proteins that are both rich in nutrients and sustainably produced need to be explored, as the global demand for protein for human consumption continues to increase. Examples of alternative proteins that potentially may be used in human nutrition include cereals, edible insects, algae, fungi, and cultured meat, all of which can offer good nutritional value, but need to be further explored (Malila et al., 2024). Among these alternative sources, seaweeds have gained significant attention due to their high protein and polysaccharide content, abundance of bioactive compounds, and potential functional benefits (Lomartire & Gonçalves, 2022). Seaweeds, or marine macroalgae, are classified into three major groups: Rhodophyta (red algae), Phaeophyta (brown algae), and Chlorophyta (green algae), each exhibiting unique biochemical composition and nutritional properties (Salehi et al., 2019). Red seaweeds are rich in polysaccharides like carrageenans and agar, whereas brown seaweeds contain alginate, fucoidan, and laminarin (Ye et al., 2023), and green seaweeds primarily contain cellulose, along with sulphated polysaccharides such as ulvans, in their cell walls (Domozych et al., 2012). The gelling properties of seaweed polysaccharides can be utilised for a wide range of applications in the food, biomedical, pharmaceutical, and biotechnology industries (Xie et al., 2024).

These seaweed-derived polysaccharides also offer nutritional benefits, as they act as dietary fibres (i.e., resistant to digestion by human digestive enzymes), contributing to gut health by modulating intestinal viscosity, delaying nutrient absorption, and influencing microbial fermentation in the colon (You et al., 2020). However, seaweed polysaccharides can influence the digestive fate of proteins (Díaz-Piñero

* Corresponding author.
E-mail address: marta.martinez@csic.es (M. Martínez-Sanz).

https://doi.org/10.1016/j.foodres.2026.119614
Received 20 January 2026; Received in revised form 26 May 2026; Accepted 1 June 2026
Available online 2 June 2026

et al., 2026). Due to their ability to form gels, they associate with proteins, which may reduce their susceptibility to being hydrolysed by digestive enzymes, reducing and/or delaying proteolysis (Vasconcelos et al., 2023). As a result, these polysaccharides may not only modify digestion kinetics but also reshape the micro- and nano-scale structures that emerge during gastrointestinal breakdown. As an example, carrageenans form gel-like networks that have been reported to slow proteolysis and influence amino acid release kinetics (Xie et al., 2024) and alginate–protein aggregates resist gastric digestion by inhibiting proteolytic enzymes, altering the delivery of peptides to the small intestine (Chater et al., 2015). Some dietary fibres exhibit bile salt binding capacity, contributing to cholesterol reduction and potentially affecting the micellization and transport of nutrients (Díaz-Piñero et al., 2024; Massa et al., 2022). These physicochemical interactions influence how macronutrients self-assemble during digestion, potentially giving rise to colloidal structures, fibre-rich aggregates, or residual nanodomains. Fibre–bile salt interactions may influence the nanoassembly of digestion products in the gut. In particular, some polysaccharides either stabilise or hinder the formation of ordered lamellar/micellar structures in gastrointestinal digesta (Díaz-Piñero et al., 2024). However, the exact mechanisms by which these polysaccharides interact with proteins and influence the digestion process are still not fully understood and require further exploration.

Whereas *in vitro* models have been extensively applied to study the gastrointestinal digestion of a variety of protein-polysaccharide systems (Díaz-Piñero et al., 2024; Štreimikytė et al., 2020), they do not fully capture the dynamic conditions of the gastrointestinal tract.

Importantly, several key aspects could not be addressed in our previous *in vitro* study (Díaz-Piñero et al., 2026), including the contribution of endogenous proteins to the peptide pool, the dynamic secretion and reabsorption of bile salts, and the formation of digestion structures under physiologically relevant conditions. In addition, *in vitro* systems also lack inter-individual variability and may not fully reproduce the extent of digestion achieved *in vivo*. Therefore, it remains unclear whether the structural effects and interactions observed *in vitro* are preserved, modified, or overridden under physiological conditions.

In this regard, the pig model is widely used in dietary research to study nutrient digestion and absorption at the ileal level, owing to its anatomical and physiological similarities to the human gastrointestinal tract (Hodgkinson et al., 2022; Rowan et al., 1994; Stein, 2024). Sampling of ileal digesta in pigs allows for the precise determination of the digestibility and bioavailability of dietary components before they undergo fermentation in the large intestine (Hodgkinson et al., 2022). There is, however, a lack of knowledge about whether or not these models can replicate the micro- and nanostructures generated during digestion, especially when fibre-rich matrices are present. This knowledge gap is critical, since the assembly of digestive products may influence nutrient transport, interaction with bile salts, and metabolic responses. To address these limitations, this study provides, for the first time, a multiscale structural characterisation of ileal digesta under *in vivo* conditions, integrating complementary structural and physicochemical techniques.

We hypothesised that seaweed-derived polysaccharides modulate protein digestion not only by altering proteolysis kinetics, but also by influencing the micro- and nano-scale assembly of digestion products in the gastrointestinal tract. Accordingly, the objective of this study was to investigate the role of seaweed polysaccharides in shaping gastrointestinal digestion and nanoassembly of model food proteins (casein and whey proteins) using an *in vivo* pig model. Particular attention was given to the formation of multi-scale structures within the complex food matrix, including the contribution of other dietary components such as starch, which may influence the physicochemical environment during digestion.

2. Materials and methods

2.1. Materials

Six ingredients were used to formulate the experimental diets. Micellar casein powder (PRODIET 85B) (76.9% protein, 5% carbohydrates, 7.5% ash, 1.5% fat and 5% moisture, as specified by the provider) and whey protein isolate powder (PRODIET 90S) (84.3% protein, 5.5% carbohydrates, 2.5% minerals, 1% fat and 5.5% moisture, as specified by the provider), purchased from Ingredia S.A. (Arras, France), were used as the two protein sources. The selected polysaccharides were commercial agar (ROKOAGAR® RGM 900), alginate (ROKOGEL® 20,800), carboxymethylcellulose (ROKOGEL® 25,300), and carrageenan (ROKOGEL® 4601), supplied by Industrias Roko (Asturias, Spain). Agar (ROKOAGAR® RGM 900) is a refined food-grade polysaccharide. According to the manufacturer's specifications, this product exhibits a high gel strength (~900 g/cm^2), low ash content (<5%), and low moisture content (<15%). As a natural polysaccharide, agar presents a molecular weight distribution typically in the range of 120–200 kDa, depending on the source and extraction conditions. Alginate, carrageenan, and carboxymethylcellulose (CMC) were also used as commercial food-grade polysaccharides with well-defined thickening or gelling properties. While detailed molecular parameters such as molecular weight distribution or degree of substitution were not fully specified by the supplier, these materials are representative of industrial ingredients and were selected to reflect realistic formulation conditions.

2.2. Experimental diets

Ten experimental diets were formulated using casein (CAS) or whey protein isolate (WPI) as the main protein sources. Casein was used either without mixing with polysaccharides or in a 75:25 ratio with agar, alginate, carrageenan, or carboxymethyl cellulose. Casein was also used in a 50:50 and a 25:75 mixture with agar. Whey protein isolate was used either without mixing with polysaccharides or in a 75:25 ratio with agar. A detailed explanation of how the diets were formulated is published elsewhere (Fanelli et al., 2026) and in Table S1. In addition to the protein–polysaccharide blends, a nitrogen-free (N-free) diet was prepared to quantify basal endogenous nitrogen and amino acid losses, as well as to evaluate the structural organisation of the ileal digesta in the absence of dietary protein. Titanium dioxide was used in all diets as an indigestible marker to enable digestibility calculations (Fanelli et al., 2026). Representative samples of each raw ingredient and final diets were collected for chemical composition analyses.

2.3. In vivo gastrointestinal digestions

The animal experiment protocol was reviewed and approved by the Institutional Animal Care and Use Committee (IACUC) of the University of Illinois at Urbana-Champaign (IL, USA) (approval number #21244), and the *in vivo* experiments were conducted at the University of Illinois using nine growing pigs (initial body weight: 25.7 ± 1.4 kg). All pigs were surgically fitted with a T-shaped cannula made of stainless steel, positioned 10 cm proximal to the ileocecal junction in the distal ileum (Stein et al., 1998). After surgery, pigs underwent a 7-day recovery period during which feed intake was gradually increased to allow for full gastrointestinal recovery and to prevent overloading the digestive system. Pigs were housed individually in temperature- and humidity-controlled pens with free access to water throughout the experiment. Feeding occurred twice daily, and feed allowance was adjusted based on metabolic body weight (Latimer et al., 2023).

Each of the nine pigs received six experimental diets using a 9 × 6 incomplete Latin square design with the 9 protein-containing ingredients and 6 seven-day periods. All pigs were fed the N-free diet in the middle of the experimental periods. The initial five days of each period served as an adaptation phase to the diet, whereas ileal digesta were

collected on days 6 and 7 for 9 h per day, beginning immediately after the feeding of the morning meal. Digesta collection followed standard operating procedures (Espinosa et al., 2022; Fanelli et al., 2026; Hodgkinson et al., 2022). Following this experimental design, 6 ileal digesta samples were collected from 6 different pigs fed each experimental diet. However, for the N-free diet, 9 ileal digesta samples from different pigs were collected because all 9 pigs were fed the N-free diet in one period. Table 1 shows the sample codes assigned to the collected samples.

2.4. Compositional analysis of the ileal digesta

Ileal digesta samples were kept frozen for structural analyses, while a fraction was freeze-dried and finely ground for compositional analyses. Dry matter was determined using AOAC method 927.05 (Latimer et al., 2023), whereas nitrogen was determined by combustion using AOAC method 990.03, performed on a LECO FP628 analyser (LECO Corp., Saint Joseph, MI, USA). Crude protein (CP) was calculated as nitrogen × 6.25. Ash was analysed following the AOAC Official Method 923.03. Total lipid content was determined following the Folch method with minor modifications (Lomartire & Gonçalves, 2022). Briefly, 30 mg of the sample was suspended in 200 μL of Milli-Q water and transferred to a 10 mL glass tube. Methanol (1.66 mL) was added, and the mixture was stirred at 1400 rpm for 10 min. Subsequently, 3.32 mL of dichloromethane was added, and mixing continued for an additional 20 min. Afterwards, 1 mL of 20 mM acetic acid was added, and the sample was agitated for an additional 10 min. The mixture was centrifuged to separate the phases, and the lower organic layer was carefully collected. The aqueous phase was re-extracted with 1.66 mL of dichloromethane, and both organic phases were combined. The pooled extract was filtered through a glass syringe fitted with a 0.45 μm filter, and the solvent was evaporated to dryness. The total lipid content was quantified gravimetrically.

2.5. Determination of total starch in ileal digesta

Total starch in the ileal digesta was determined using the Total Starch Assay Kit (AA/AMG; Megazyme, Ireland, cat. # K-TSTA-100 A), according to the manufacturer's instructions, with minor adaptations for samples potentially containing free glucose (Megazyme, 2009).

Table 1
Sample codes of the ileal digesta obtained from the different diets.

Sample code	Protein Source	Polysaccharide	Protein (% w/w)	Polysaccharide (% w/w)
CAS	Casein	–	100	0
CAS/AG-25	Casein	Agar	75	25
CAS/AG-50	Casein	Agar	50	50
CAS/AG-75	Casein	Agar	25	75
CAS/ALG-75	Casein	Alginate	25	75
CAS/CEL 75	Casein	Carboxymethyl cellulose (CMC)	25	75
CAS-CAR-75	Casein	Carrageenan	25	75
WPI	Whey protein isolate	–	100	0
WPI/AG-75	Whey protein isolate	Agar	25	75
N-free	–	–	–	–

2.6. Polyacrylamide gel electrophoresis (SDS-PAGE)

SDS-PAGE was employed to analyse the molecular weight distribution of proteins present in the ileal digesta. The sample loading buffer consisted of Tris-HCl buffer, 1.6% SDS, 8% glycerol, 0.002% Bromophenol Blue, and 2% β-mercaptoethanol, and was used to dissolve the samples. The samples, prepared at a protein concentration of 2 mg/mL, were heated at 95 °C for 5 min in a thermoblock to ensure denaturation. A volume of 40 μL from each sample was loaded into the wells of a precast gel (Criterion XT 12% Bis-Tris polyacrylamide gel, Bio-Rad). A molecular weight marker (Precision Plus Protein™ Unstained Standard, Bio-Rad) was included as a reference. Electrophoresis was conducted in the Criterion electrophoresis cell (Bio-Rad) at a constant voltage of 150 V, using a running buffer prepared by diluting 20× XT MES buffer with Milli-Q water in a 19:1 ratio. After electrophoresis, the gel was rinsed with Milli-Q water, and the protein bands were stained with Instant Blue Coomassie dye (Expedeon Protein Solutions, Harston) for 1 h, followed by an overnight incubation for complete staining.

2.7. Peptidomic analysis

Peptide profiling of ileal digesta was carried out by tandem mass spectrometry using a Vanquish Neo UHPLC system (Thermo Scientific, Germany) coupled to an Orbitrap Exploris 240 mass spectrometer (Thermo Scientific, USA). Before analysis, samples containing approximately 10 μg of protein were prepared in 8 M urea and 0.1 M ammonium bicarbonate (final volume 20 μL). Disulfide bonds were reduced with 2 μL of 0.1 M dithiothreitol (DTT) at 37 °C for 1 h (700 rpm) and alkylated with 2 μL of 0.5 M iodoacetamide for 45 min in the dark at room temperature. The samples were then diluted with 55.5 μL of LC/MS-grade water and digested overnight at 37 °C with sequencing-grade trypsin at a 1:20 enzyme-to-protein ratio (*w*/w). The digests were evaporated to dryness, resuspended in 0.1% trifluoroacetic acid (TFA), and centrifuged at 15.000 rpm for 5 min. Peptides were purified using C18 Ziptip devices (Millipore, USA) that were preconditioned with 50:50 acetonitrile/water containing 0.1% TFA, equilibrated with 0.2% TFA, and eluted in 50:50 acetonitrile/water +0.1% TFA. The eluates were dried under vacuum and reconstituted in 12 μL of 0.1% formic acid; 1 μL was injected for UHPLC–MS/MS analysis. Peptides were separated on a C18 column (150 × 2.1 mm, 1.7 μm) using a gradient from 0 to 95% solvent B (80,20 acetonitrile/water +0.1% formic acid) over 64 min at 0.3 $\mu L min^{-1}$, with solvent A consisting of water +0.1% formic acid. The Orbitrap Exploris 240 operated in positive ion mode, acquiring full mass spectra (MS) scans over an m/z range of 350–1550 at 120000 resolutions, with radio-frequency lens at 70%, normalised automatic gain control (AGC) target of 300%, and an intensity threshold of 3.0×10^4. The MS/MS spectra were obtained at a resolution of 30000 using a 2 Da isolation window, normalised AGC target of 50%, and normalised higher-energy collisional dissociation (HCD) collision energy of 30%. Spectra were analysed using PEAKS Studio 11 (Bioinformatics Solutions Inc.) for de novo sequencing and database matching against in-house protein libraries containing bovine casein variants and porcine endogenous proteins. Search parameters were set to trypsin digestion, up to two missed cleavages, carbamidomethylation (Cys) as a fixed modification, oxidation (Met) as a variable modification, and precursor and fragment tolerances of 10 ppm and 0.02 Da, respectively.

2.8. Relative protein contribution

The relative contribution of dietary and endogenous proteins to the ileal peptide was calculated based on summed peptide ion areas as follows:

$$\%Dietary\ proteins = \frac{\Sigma\ Dietary\ peptide\ area}{\Sigma\ Total\ peptide\ area} x100 \quad (1)$$

$$\%Endogenous\ proteins = \frac{\Sigma\ Endogenous\ peptide\ area}{\Sigma\ Total\ peptide\ area} x100 \quad (2)$$

where total peptide area corresponds to the combined ion areas of all identified peptides in each sample.

2.9. Structural characterisation of diets and ileal digesta

2.9.1. Confocal laser scanning microscopy (CLSM)

The structural characteristics of both diets and ileal digesta samples obtained from pigs were examined using confocal laser scanning microscopy (CLSM). Imaging was conducted with a Zeiss LSM800 confocal system, integrated with the Axio Imager 2 upright microscope (Zeiss, Germany) and operated via ZEN Blue 3.4 software. For visualisation, two staining agents were simultaneously used: SCRI (SR2200) (SCRI Renaissance 2200 staining, Martin Bayer) at a concentration of 0.1% to stain carbohydrates, and Fast Green (Fast Green FCF-Dye content ≥85%, Sigma) at a concentration of 0.1% to stain proteins and starch. Samples were directly placed on microscope glass slides and covered with cover slips for imaging. Microscopic analysis was performed using a 40× objective lens with a numerical aperture (NA) of 0.7, with excitation provided by a HeNe laser. Fluorescence emission was detected at wavelengths of 350–405 nm for SR2200 (carbohydrates) and 635–647 nm for Fast Green (proteins and starch). Images were processed using the ImageJ-win64 Fiji Software.

2.9.2. Transmission Electron microscopy (TEM)

Ileal digesta samples were centrifuged and diluted 1:10 in Milli-Q water, and a 2 μL aliquot was stained with uranyl acetate to enhance protein contrast. The sample was then deposited onto a collodion-coated carbon grid and air-dried. Transmission electron microscopy (TEM) was performed using a JEM-1010 microscope (JEOL, 1992), equipped with a thermionic emission gun with a tungsten filament, operating at an accelerating voltage of up to 100 kV. The system included a high-contrast lens (SAP-10B pole piece) with an interline resolution of 0.2 nm, and observations were conducted using a 10× objective. Particle size distributions were determined by image analysis with the Fiji (ImageJ-win64) software package.

2.9.3. Small-angle X-ray scattering (SAXS)

SAXS assays were carried out in the Non-Crystalline Diffraction beamline, BL-11, at the ALBA synchrotron light source (www.albasynchrotron.es). The initial ingredients, the diets and their corresponding ileal digests were placed into 2 mm quartz capillaries (Hilgenberg GmbH, Germany) and sealed before being analysed. The energy of the incident photons was 12.4 keV or, equivalently, a wavelength, λ, of 1 Å. The SAXS scattering patterns were collected using a photon counting detector, Pilatus 1 M, with an active area of 168.7 × 179.4 mm^2, an effective pixel size of 172 × 172 μm^2 and a dynamic range of 20 bits. The sample-to-detector distance was set to 6700 mm, resulting in a q range with a maximum value of q = 0.2 $Å^{-1}$. An exposure time of 8 s was selected based on preliminary trials. The data reduction was treated by pyFAI Python code (ESRF), modified by ALBA beamline staff, to do online azimuthal integrations from a previously calibrated file (Kieffer & Wright, 2013). The calibration files were created from a silver behenate (AgBh) standard. The intensity profiles were plotted as a function of the scattering vector (q) using OriginLab 2024 (OriginLab Corporation, Northampton, MA, USA), which was employed for data visualisation and basic analysis.

2.10. Viscosity measurements

Ileal digesta samples were thawed on ice and centrifuged at 4000 ×*g* for 10 min to obtain the liquid supernatant. Viscosity measurements were performed using a modular compact rheometer (MCR 302e, Anton Paar, Austria) equipped with a parallel-plate geometry (upper plate PP50–1, 60 mm diameter; lower plate 62 mm) and a solvent trap to prevent evaporation. The measurement gap was set to 0.5 mm. Approximately 2 mL of digesta supernatant was loaded into the temperature-controlled stage (37 °C) and equilibrated for 1 min before measurement. Steady-shear flow curves were recorded over a logarithmically increasing shear rate ($\dot{\gamma}$, s^{-1}) from 0.01 to 1000 s^{-1} at 37 °C, mimicking physiological conditions. Apparent viscosity (η, mPa·s) was obtained as a function of shear rate. All measurements were performed in triplicate, using a freshly loaded aliquot for each run.

2.11. Determination of bile salts

Bile acid levels were measured from 10 μL of sample, diluted with an equal volume of water, using a bile acid assay kit (Sigma-Aldrich, USA; Cat. #MAK309). This fluorometric method offers a straightforward approach to quantifying total bile acids in biological samples. The assay relies on the enzyme 3α-hydroxysteroid dehydrogenase, which reacts with all 12 major bile acids, converting NAD to NADH and reducing a probe to generate a highly fluorescent product. The resulting fluorescence (excitation at 530 nm, emission at 585 nm) is directly proportional to the bile acid concentration in the sample.

2.12. ζ-Potential and particle size analysis

The hydrodynamic diameter and ζ-Potential were measured in diets and ileal digesta samples. To prepare samples, 10 mL suspensions were made by dissolving the dried samples at a 1:100 ratio in Milli-Q water, and the resulting supernatant was used for analysis. Subsequently, 700 μL of the liquid was transferred into a polycarbonate capillary cell DTS 1070, equipped with two gold-laminated electrodes (Malvern Instruments, UK). The zeta potential and hydrodynamic diameter were then measured using a Nano ZS Dynamic Light Scattering Analyser (Malvern, UK).

2.13. Statistical analysis

Normality of residuals was assessed using the Shapiro–Wilk test, and homogeneity of variances was evaluated using Levene's test. For protein, ash, and carbohydrate data, the assumption of variance homogeneity was violated; therefore, Welch's ANOVA followed by Games–Howell post hoc testing was applied. Variables meeting the homogeneity assumption were analysed using ordinary one-way ANOVA with Tukey's post hoc test. Statistical significance was set at $p < 0.05$.

3. Results and discussion

3.1. Chemical composition of the ileal digesta

The composition of the ileal digesta from pigs fed the experimental diets is summarised in Table 2. Clear differences were observed among formulations, reflecting the varying protein-to-polysaccharide ratios and the distinct physicochemical characteristics of each dietary fibre. Moisture levels showed wide variation (6–21%, $p < 0.01$), consistent with the differing water-holding capacities of the fibres added in the diets. The highest humidity was observed for the digests from the diets containing agar (CAS/AG-25, CAS/AG-50, and CAS/AG-75), indicating strong water retention in these samples, which may be due to a high amount of highly hygroscopic agar remaining in the digests. Agar-based hydrogels can absorb and retain water up to at least an order of magnitude higher than their own dry weight, with chemically cross-linked agar–acrylic acid systems reaching swelling ratios in the range of several thousand percent of their dry mass while maintaining structural integrity (Chaudhary et al., 2020). Studies comparing dietary fibres confirm that agar typically has a higher water holding capacity (WHC) than many other food polysaccharides, such as cellulose, due to its unique linear structure and capacity to form rigid, interwoven junction zones with water molecules. In protein–agar systems, the presence of

Table 2
Gross composition of ileal digesta. Values correspond to the averages calculated from different pigs[†].

	Humidity (%)	Protein (%)	Ash (%)	Lipids (%)	Carbohydrates (%)[*]
CAS	11.1 ± 1.1^{bc}	14.6 ± 0.7^{a}	21.3 ± 2.7^{a}	8.4 ± 1.0^{b}	44.5 ± 3.2^{a}
CAS/AG-25	21.1 ± 0.4^{a}	15.2 ± 3.1^{a}	23.0 ± 2.9^{a}	4.91 ± 0.06^{cd}	41.7 ± 4.3^{a}
CAS/AG-50	19.6 ± 0.9^{ab}	11.9 ± 0.4^{a}	12.3 ± 0.2^{a}	7.0 ± 1.0^{bc}	49.1 ± 1.4^{a}
CAS/AG-75	20.4 ± 3.1^{ab}	8.9 ± 5.1^{a}	13.2 ± 1.4^{a}	5.9 ± 0.6^{cd}	51.6 ± 6.2^{a}
CAS/ALG-75	10.4 ± 0.9^{bc}	8.7 ± 4.5^{a}	13.3 ± 6.3^{a}	5.3 ± 1.2^{cd}	62.3 ± 7.8^{a}
CAS/CEL-75	12.1 ± 1.4^{bc}	4.9 ± 1.6^{a}	10.7 ± 4.6^{a}	6.2 ± 0.3^{cd}	66.1 ± 5.1^{a}
CAS/CAR-75	10.7 ± 3.2^{c}	7.6 ± 0.6^{a}	16.3 ± 8.1^{a}	3.92 ± 0.05^{d}	61.5 ± 8.7^{a}
WPI	9.7 ± 1.6^{c}	25.3 ± 1.0^{a}	10.35 ± 0.09^{a}	7.10 ± 0.02^{bc}	47.5 ± 1.6^{a}
WPI/AG-75	16.4 ± 2.0^{bc}	8.9 ± 1.3^{a}	13.4 ± 3.0^{a}	5.6 ± 0.2^{cd}	55.7 ± 3.8^{a}
N-free	6.9 ± 1.1^{c}	22.7 ± 1.2^{a}	15.4 ± 1.6^{a}	11.4 ± 0.4^{a}	44.0 ± 2.3^{a}
SEM	2.41	3.93	3.92	0.62	7.54
p-value	<0.01	0.57	0.404	<0.001	0.236

[*] Carbohydrates were calculated as the difference between the remaining mass and the mass balance.

[†] Values are expressed as mean ± SD (n = 2). Different superscript letters within the same column indicate significant differences among formulations ($p < 0.05$). Humidity and lipid data were analysed using one-way ANOVA followed by Tukey's post hoc test, whereas protein, ash, and carbohydrate data were analysed using Welch's ANOVA followed by Games–Howell post hoc testing. Compositional analyses are presented as indicative values to support structural interpretation and were not used as the primary basis for statistical inference.

agar leads to the formation of gels with exceptionally high WHC, up to 48–92%, when compared to systems without agar (Paleekui et al., 2025).

Protein content of the ileal digesta ranged from approximately 5% to 25% and showed no statistically significant differences among diets, although a tendency was observed. The highest protein levels were detected in the N-free and WPI digests. Notably, the higher protein content observed in the N-free digesta compared with the CAS diet suggests that endogenous protein secretion may have been influenced by diet composition. In contrast, digesta obtained from diets containing polysaccharides tended to display lower protein proportions, reflecting the greater contribution of non-digested polysaccharides to the overall digesta mass. Ash content varied between approximately 10% and 23%, but did not differ significantly among formulations. Lipid content, however, was significantly affected by diet formulation ($p < 0.001$), with values ranging from approximately 4% to 11%. The highest lipid level was observed in the N-free digesta, whereas the lowest lipid content was detected in CAS/CAR-75, highlighting formulation-dependent differences in lipid recovery within the ileal digesta.

3.2. Analysis of the protein fraction in the ileal digesta

SDS-PAGE analysis was conducted to determine the molecular weight distribution of the proteins in the different diets and evaluate the presence of protein fragments in the corresponding ileal digesta. For the diets (Fig. 1, top panel), distinct protein bands were consistently observed, corresponding to the two protein ingredients, CAS and WPI. In particular, for the diets containing CAS as the protein source, prominent bands were detected within the 19–35 kDa range, which align with the molecular weights of casein subtypes: α-casein (~29–30 kDa), β-casein (~24–25 kDa), and κ-casein (~19–21 kDa) (Hu et al., 2025). On the other hand, in the diets containing WPI, additional characteristic bands were identified for β-lactoglobulin (18.4 kDa), α-lactalbumin (14.2 kDa), and potentially lactoferrin (~80 kDa), as well as bovine serum albumin (~66 kDa) (Farrell et al., 2004). Casein characteristic bands were also observed, as WPI contains a proportion of casein (76.9% of dry matter according to the provider) along with the whey proteins. The final lane of the gel, representing the nitrogen-free control, exhibited no visible protein bands, as expected.

The bottom panel of the SDS-PAGE gel displays representative ileal digesta samples collected from pigs fed the respective diets. These lanes provide insight into the presence of residual proteins or peptides that were not absorbed in the small intestine. One representative ileal digesta sample per diet is shown, selected from the two analysed samples based on the similarity of protein banding patterns between replicates. Overall, all digesta samples from pigs fed the same diet exhibited comparable protein banding profiles, as shown in Fig. S1. As observed, the characteristic bands from the proteins present in the initial diets were no longer visible in the ileal diets, indicating that these were efficiently hydrolysed by gastrointestinal enzymes. Although several bands were visible within the 20–60 kDa range, these were also visible in the digest from the N-free diet, suggesting that they correspond to endogenous proteins that were secreted during the digestion process. These digestive enzymes comprise trypsin (~24 kDa), chymotrypsin (~25 kDa), carboxypeptidase B (~35 kDa), and amylase (~55–60 kDa) (Ávila-Arres et al., 2024). In addition, sloughed epithelial cell proteins such as actin (~42 kDa), tubulin (~50–55 kDa), and villin (~95 kDa) may contribute to the observed bands, along with immunoglobulin fragments (e.g., IgA heavy chain ~55 kDa, light chain ~25 kDa), which are commonly found in mucosal secretions (Ayllón et al., 2017; Mamone & Picariello, 2023). Similar observations have been reported in studies evaluating *in vivo* protein digestibility in pigs, where SDS-PAGE of ileal or duodenal contents revealed the presence of endogenous proteins after digestion of dairy-based formulations (Egger et al., 2019). The analysis was performed on the solid fraction extracted from the ileum, which represents the non-absorbed dietary components. Therefore, the absence of milk protein bands is expected, as proteins that are efficiently digested and absorbed should not be present at this stage. Indeed, the true ileal digestibility of milk proteins is among the highest reported for dietary proteins, close to 100% (Bos et al., 2003; Fanelli et al., 2026). Although dietary fibres such as agar, alginate, carrageenan and cellulose have been shown to delay the digestion of milk proteins *in vitro* (Díaz-Piñero et al., 2026; Fontes-Candia et al., 2023), our results indicate that they do not prevent proteolysis during the intestinal phase. Importantly, while SDS-PAGE detected no intact proteins, extensive proteolysis was evidenced by the presence of milk-derived peptide fingerprints, as confirmed by peptidomic analysis.

Proteins bound to the non-digestible polysaccharides or protein fractions with molecular weights <10 kDa could not be properly detected by SDS-PAGE. Thus, peptidomic analyses were performed on one ileal digesta sample per diet to assess differences in ileal peptide profiles. A total of 245 peptides corresponding to 11 different proteins were identified in the ileal digesta of pigs fed the N-free diet (Table S2). The most abundant endogenous proteins detected, such as digestive enzymes (e.g., trypsin, chymotrypsin, carboxypeptidase A and B) and mucins, have been previously reported as part of the basal endogenous protein profile in ileal digesta of pigs (Ávila-Arres et al., 2024).

When the relative contribution of proteins was examined, peptides coming from endogenous proteins clearly dominated in all the samples. In the CAS digesta (Tables S3-S4), they represented about 98.7% of the total signal, while milk-derived proteins accounted for 1.3%. Very similar values were obtained for CAS/AG-75 (98.6% vs 1.4%) (Tables S5-S6) and CAS/ALG-75 (98.9% vs 1.1%) (Tables S7-S8). The

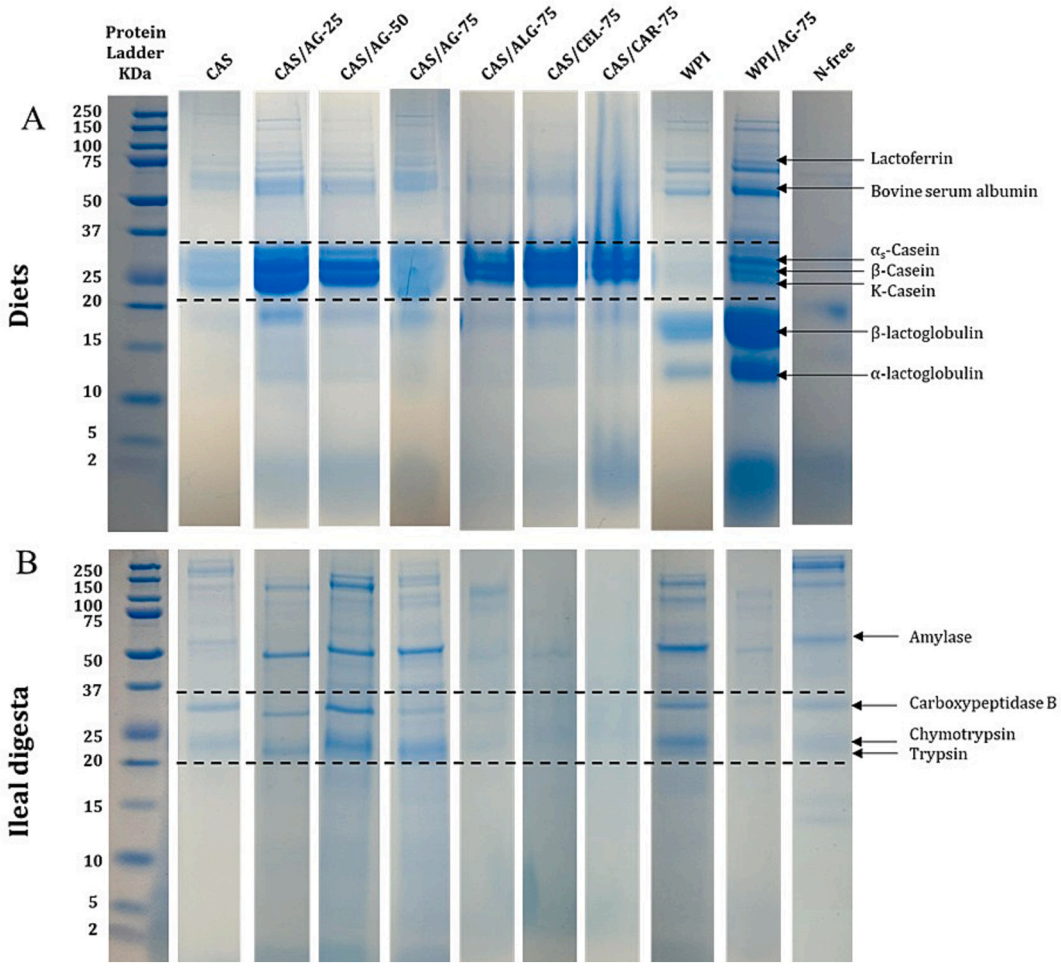

Fig. 1. SDS-PAGE protein profiles of (A) initial diets and (B) their corresponding ileal digesta. Representative samples from selected pigs are shown in Fig. 1B.

CAS/CEL-75 digest (Tables S9-S10) showed the smallest proportion of milk-derived proteins (0.02%). In CAS/CAR-75 (Tables S11-S12), peptides from endogenous proteins made up 98.4% of the total, with milk proteins accounting for 1.6%. A comparable pattern was observed for the WPI diets. In WPI, milk-derived peptides from dietary proteins represented only 0.06% (Tables S13-S14), and in WPI/AG-75, around 0.27% (Tables S15-S16). Notably, the WPI/AG-75 diet showed a clear enrichment of milk-derived peptides in the ileal digesta compared with WPI alone. Although the absolute values remained low, this increase indicates that the WPI–agar matrix partially protected specific whey protein domains from complete hydrolysis and absorption in the upper gastrointestinal tract. Still, the true ileal digestibility was not statistically reduced (Fanelli et al., 2026). The N-free digesta, as expected, contained exclusively peptides from endogenous proteins (99.6%), derived from digestive secretions and epithelial shedding. Focusing on the identified dietary peptides, the samples CAS/ALG-75 and CAS/CAR-75, followed by CAS/AG-75, showed some unique peptide sequences, indicating that specific regions of milk proteins were partially protected from complete enzymatic hydrolysis in the upper gastrointestinal tract. This localised protection likely resulted from interactions with dietary fibres, allowing a small number of peptide fragments to persist in the ileum. Importantly, this effect was limited to discrete protein domains and did not contradict the overall extensive digestion and absorption of milk proteins, as evidenced by the very low proportion of milk-derived peptides detected in the ileal digesta. These observations indicate that the milk proteins in the diets had been extensively hydrolysed and largely absorbed in the upper gastrointestinal tract, and therefore, they were not present in the ileum. However, the presence of dietary fibres like agar, alginate, and carrageenan might have protected specific protein domains to a small extent. The analysis was performed after trypsinisation of the samples to investigate the insoluble protein fraction at this level. In addition, under our analytical conditions, only peptides longer than 5 amino acids are detected, and thus, the presence of shorter peptides from milk proteins cannot be excluded.

Despite the differences observed among formulations in the residual peptide fingerprints, the overall results indicate that both casein and whey proteins were extensively hydrolysed and largely absorbed before reaching the ileum. At first glance, this could suggest that fibre–protein interactions have limited physiological relevance in this system. However, such an interpretation would overlook the dynamic nature of gastrointestinal digestion. Ileal digesta provide only an endpoint view of the process and do not capture transient effects occurring during the gastric and early intestinal phases, where dietary fibres may influence enzyme accessibility, matrix disintegration, and the kinetics of proteolysis. Indeed, previous studies have shown that dietary fibres can alter proteolysis kinetics by modifying digesta viscosity, restricting enzyme diffusion, delaying matrix disintegration and limiting enzyme accessibility to protein substrates (Mackie et al., 2016). Such effects have been reported for a range of protein–polysaccharide systems, where slower protein hydrolysis and altered peptide release patterns were observed despite little or no change in the final extent of digestion (Díaz-Piñero et al., 2026). Changes in proteolysis kinetics may be physiologically relevant because they influence the timing and location of amino acid release within the gastrointestinal tract, which can affect subsequent nutrient utilisation and postprandial responses (Singh et al., n.d.; Boirie et al., 1997). The present results suggest that seaweed polysaccharides

primarily affect these dynamic aspects of digestion rather than the final extent of protein hydrolysis measured at the ileal level.

3.3. Viscosity of the ileal digesta

The presence of non-digested polysaccharides in the digests was expected to affect their rheological properties. The apparent viscosities of the liquid fractions from representative ileal digesta (the same samples used for SDS-PAGE analysis) are shown in Fig. 2. All samples exhibited clear shear-thinning (pseudoplastic) behaviour, where viscosity progressively decreased with increasing shear rate. Such rheological behaviour is typical of complex biopolymer dispersions, where the partial alignment and disentanglement of macromolecular chains under flow reduce intermolecular friction and flow resistance (Wu et al., 2016). This observation is also consistent with previous studies showing that hydrocolloids and dietary fibres can modulate starch digestion kinetics and postprandial glycaemic response through multiple mechanisms. These include increased viscosity, which limits enzyme mobility, reduced diffusion of digestive enzymes and substrates, and the formation of physical barriers that restrict enzyme access to starch granules (Brennan, 2005; Dikeman & Fahey Jr., 2006).

The digesta from the pigs fed the N-free diet had the lowest viscosity values among all samples (≈ 10–100 mPa·s), confirming that the soluble components in the digesta in the absence of non-digestible polysaccharides contributed minimally to the viscosity. Similarly, CAS and WPI, which contained only protein as the structural component, had comparatively low viscosities, consistent with limited network formation. In contrast, the protein-polysaccharide diets produced markedly different profiles depending on the polysaccharide incorporated. CAS/CEL-75, CAS/AG-50, and CAS/CAR-75 exhibited the highest apparent viscosities, reaching values up to 10^5 mPa·s at low shear rates. Their strong shear-thinning behaviour indicates the formation of cohesive, weak-gel networks within the digesta, likely sustained by electrostatic and hydrophobic interactions between the anionic polysaccharide chains and soluble components present in the digesta (Goh et al., 2019). The viscosities of CAS/AG-75 and WPI/AG-75 could not be measured due to their gel-like consistency, indicating that strong protein–polysaccharide interactions and digestion-induced network restructuring resulted in highly structured cohesive systems with limited flowability. These two samples correspond to those with the greatest carbohydrate contents (cf. Table 1). Hence, high concentrations of agar in the digesta may have led to the formation of gel-like networks, whereas intermediate viscosities were observed for CAS/AG-25 and CAS/ALG-75, consistent with less extensive network formation.

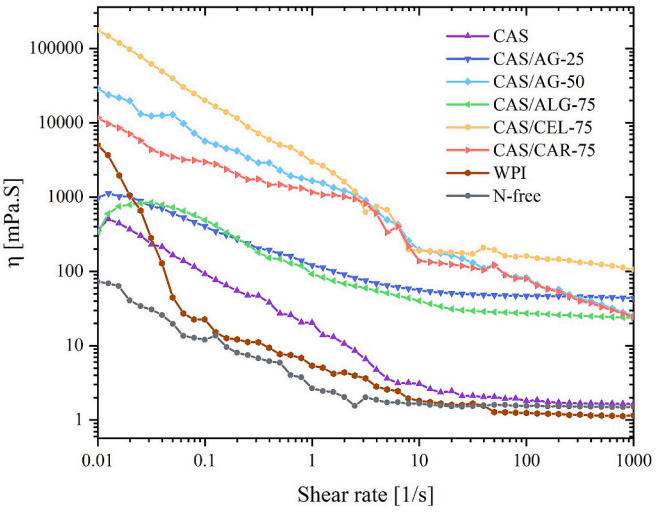

Fig. 2. Viscosity as a function of the shear rate of representative ileal digesta samples from selected pigs from each diet.

3.4. Characterisation of the micro- and nanostructural features of ileal digesta

Understanding the structural transformations produced after the gastrointestinal digestion process and the potential impact of the dietary fibres included in the diets is essential for evaluating their functional and nutritional behaviour. The microstructural changes of proteins and polysaccharides in the diets after the gastrointestinal digestion process were investigated by CLSM. Fig. 3 displays the diets (left panel) and representative ileal digesta samples with the lowest (middle panel) and highest (right panel) measured protein contents, chosen to enable qualitative comparison of digesta microstructure under contrasting protein concentrations. In the diets, a high abundance of intact corn starch granules was visible, appearing as well-defined spherical or oval structures. Such morphology is characteristic of native or lightly processed starch and aligns with previously documented granule shapes from corn starch (Van De Velde et al., 2002). In contrast, the casein and WPI protein structures were not clearly identified in the images, which is reasonable given their significantly smaller sizes; typically ~150–300 nm for casein micelles (Müller-Buschbaum et al., 2007; Sadiq et al., 2021), whereas the globular whey proteins are an order of magnitude smaller (Acharya et al., 1991). Increasing the polysaccharide content in the casein-agar formulations to 75% (CAS/AG-75 diet) resulted in the formation of a polysaccharide-rich matrix that embedded the starch granules. This matrix was not observed in the WPI/AG-75 diet, which might suggest distinct types of protein-polysaccharide interactions between agar and the two milk proteins. At the same polysaccharide inclusion level, the spatial distribution of the components in the digesta differed markedly depending on fibre type. Cellulose, similar to agar, formed a continuous matrix, whereas alginate and carrageenan were primarily associated with the surface of starch granules, with carrageenan additionally promoting granule agglomeration. This supports the existence of distinct interaction mechanisms and functional properties among the different dietary fibres.

After *in vivo* digestion, extensive degradation of starch granules was observed across most of the ileal digesta samples, as evidenced by the disappearance of well-defined granular structures. This suggests that corn starch was efficiently hydrolysed by pancreatic α-amylase and brush-border enzymes, in agreement with previous digestion studies (Jagadeesan et al., 2020). Indeed, as discussed later, the starch content in the digesta accounted for less than 1% in most cases (Table 3). Some large polysaccharide fragments were detected in the ileal digests from all the diets, including the N-free diet, which likely correspond to endogenous glycoproteins such as mucins. With regards to the protein fraction, small particles were detected in most of the ileal samples, which should correspond to endogenous proteins, as suggested by SDS-PAGE and peptidomic analyses (section 3.2). Interestingly, small protein-rich fibrillar particles were detected in the WPI/AG-75 digesta, which aligns with the peptidomic results, showing the highest proportion of milk-derived peptides found in this sample.

The nanostructure of the ingredients presents in the diets and the corresponding ileal digesta was also investigated by SAXS. The SAXS profiles of the polysaccharides in their dry state (Fig. S2A) exhibited a smooth, monotonic decay of intensity without distinct peaks or shoulders. Such featureless scattering curves indicate the absence of long-range order and suggest that the polysaccharide chains were randomly arranged within the dried matrix, lacking any residual lamellar or crystalline organisation. Similarly, the WPI powder (Fig. S2B) displayed a smooth decay in intensity without any distinctive features. In solution, β-lactoglobulin and other whey proteins exhibit characteristic shoulders or broad maxima at low to mid q values (typically $q \approx 0.05$–0.1 Å^{-1}), corresponding to their compact globular conformation and radius of gyration (Li et al., 2021). In contrast, casein showed a continuous decay in intensity, characteristic of a mass-fractal aggregate structure, and two inflexion points consistent with micellar casein structures (150–300 nm in diameter). The first inflexion point centred at $q \approx 0.04$ Å^{-1} closely

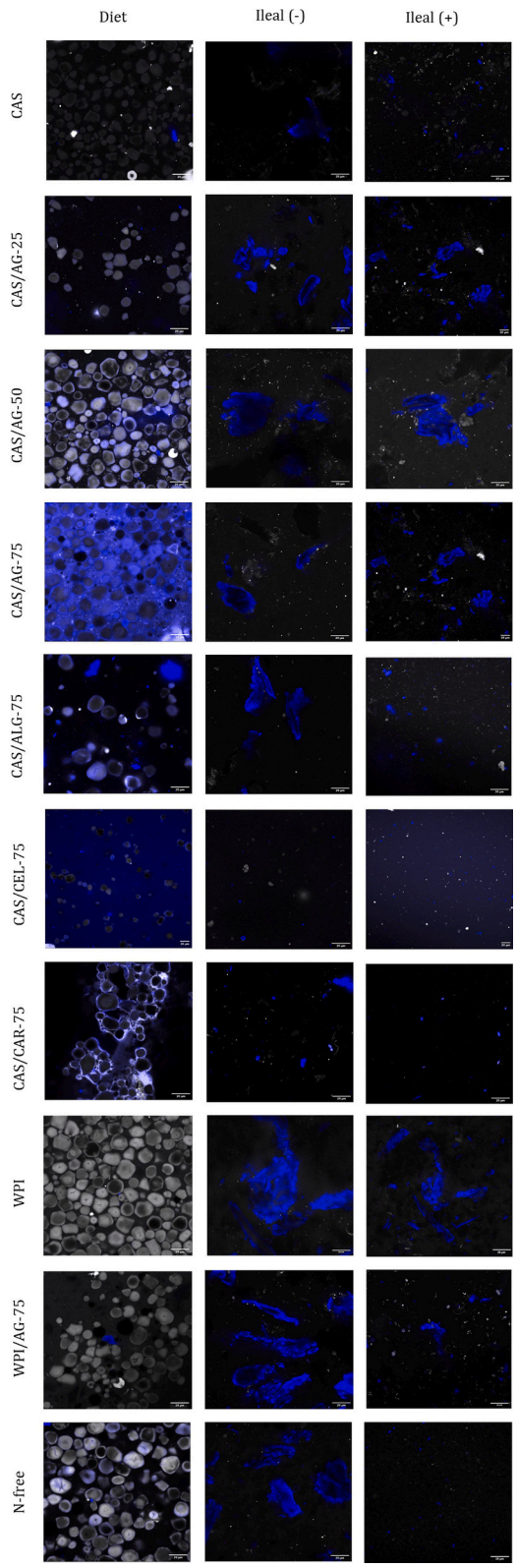

Fig. 3. Confocal Laser Scanning Microscopy (CLSM) images of the initial diets and the corresponding ileal digests from those samples containing the lowest (−) and highest (+) protein contents. Areas stained with SCRI are shown in blue (representing carbohydrates), while regions stained with Fast Green are highlighted in white (representing proteins and starch). (For interpretation of the references to colour in this figure legend, the reader is referred to the web version of this article.)

resembles that reported in previous Small-angle neutron scattering (SANS) studies, where it was attributed either to the average dimension of casein submicelles (Hansen et al., 1996) or to the characteristic spacing of calcium phosphate nanoclusters embedded within the protein matrix (Holt et al., 2003). The second broad inflexion, located at $q \approx 0.1$ $Å^{-1}$, corresponds to a feature previously noted in X-ray scattering studies and has been associated with the form factor of calcium phosphate nanoclusters interlinked within the casein matrix (Pignon et al., 2004).

Fig. 4 shows the SAXS Kratky plots of the initial diet formulations and the corresponding ileal digesta. As observed, all the diets displayed a broad scattering maximum centred at $q \approx 0.065$ $Å^{-1}$ (corresponding to $d \approx 9.7$ nm), characteristic of the lamellar spacing in semicrystalline starch, which has been widely reported in the literature (Goderis et al., 2022). The intensity and sharpness of this peak varied among diets, reflecting differences in starch concentration (Table S1) and its structural interactions with proteins and polysaccharides. In general, diets that contained higher starch proportions (such as N-free, CAS, and WPI) exhibited more defined peaks, whereas formulations enriched in polysaccharides showed broader, less pronounced maxima, indicative of partial disruption of the starch lamellar domains. It should be noted that the starch peak was more defined in CAS/AG-25 as compared to CAS, despite the slightly lower starch content in the former, which may be attributed to a higher humidity content in the CAS/AG-25 induced by the presence of agar. Indeed, water is known to promote the formation of more ordered starch at intermediate moisture contents, as evidenced by SAXS and thermal analyses in cereal and tuber starches (Kang et al., 2022).

Following digestion, most samples exhibited a marked distortion or complete disappearance of the characteristic starch lamellar peak, reflecting a substantial loss of semicrystalline order and indicating an advanced stage of enzymatic hydrolysis. This observation is fully consistent with CLSM images, which showed the near-complete degradation of starch granules and a predominance of amorphous digestion residues. In several digesta, however, a broad shoulder appeared at $q \approx 0.10$ $Å^{-1}$ (corresponding to a real-space distance of ~6.2 nm). This diffuse feature was particularly pronounced in the N-free, CAS, and WPI digests, which correspond to those with the highest starch contents in the diet formulation (Table S1). This suggests that some partially hydrolysed starch domains retaining short-range molecular order were still present in these samples. The presence of this shoulder implies that, although long-range lamellar periodicity was lost, remnants of local structural correlations persisted, possibly corresponding to clusters of partially intact double helices or to reorganised short-range aggregates formed during digestion. Similar features have been reported in SAXS and SANS studies of enzymatically or thermally processed starches (Blazek & Gilbert, 2011; Lopez-Rubio et al., 2008).

On the other hand, the absence of features characteristic of the presence of non-digested proteins in the SAXS patterns further substantiates that both WPI and CAS were extensively hydrolysed into peptides or free amino acids when reaching the ileum, without retaining higher-order supramolecular organisation, even in the presence of dietary fibres. A small peak at $q \approx 0.13$ $Å^{-1}$, corresponding to a characteristic distance of approximately 4.8 nm, was detected in the patterns from some ileal digesta from individual pigs fed with the CAS, CAS/AG-75, and CAS/ALG-75 diets, and it was consistently detected in almost all the CAS/CEL-75 diets. This feature is consistent with scattering signals previously attributed to ordered bile salt nanostructures found in *in vitro* digestion studies (Díaz-Piñero et al., 2024; Fontes-Candia et al., 2023). Its presence also aligns with previous reports describing interactions between dietary fibres and bile salts under gastrointestinal conditions (Naumann, Schweiggert-Weisz, Eglmeier, et al., 2019; Naumann, Schweiggert-Weisz, Haller, & Eisner, 2019). However, the novelty of the present work lies not in the existence of these interactions per se, but in their direct structural characterisation under *in vivo* conditions.

The presence of bile salt-related nanostructures in the SAXS profiles

Table 3
Total starch present in the ileal digesta from the different diets[‡].

	CAS	CAS/AG-25	CAS/AG-50	CAS/AG-75	CAS/ALG-75	CAS/CEL-75	CAS/CAR-75	WPI	WPI/AG-75	N-free
Resistant Starch (%)	0.83 ± 0.04^{bc}	0.14 ± 0.02^{d}	0.09 ± 0.04^{e}	0.098 ± 0.032^{e}	0.66 ± 0.01^{b}	0.099 ± 0.036^{e}	0.13 ± 0.01^{d}	0.9 ± 0.2^{bc}	0.62 ± 0.1^{b}	2.5 ± 0.4^{a}
SEM	0.16									
p-value	< 0.001									

[‡] Values are expressed as mean ± SD (n = 2). Different superscript letters indicate significant differences among diets (one-way ANOVA followed by Tukey's post hoc test, $p < 0.05$).

prompted further investigation of bile salt levels in the ileal digesta. Bile salt quantification was therefore performed for the CAS/CEL-75 samples. As shown in Fig. S3, bile salt concentrations in these samples varied from approximately 4 mM to over 17 mM, whereas the N-free digesta exhibited substantially lower levels (~1.5 mM). In particular, the CAS-3 sample showed the highest bile salt concentration, which is consistent with the more pronounced SAXS signal observed in this system.

Although the peak position remained nearly constant across all samples, its intensity and shape were variable. This suggests that in some cases, bile salts were able to organise into more defined nanostructures (narrower and more intense peaks), while in other cases, more heterogeneous structures were formed. Its appearance in the *in vivo* digesta suggests the presence of ordered bile salt structures in some pigs, which might be attributed to a reduced diffusion of mixed micelles toward the intestinal brush border, particularly under conditions of elevated digesta viscosity, and/or to increased bile salt secretion in some individuals. This effect can be attributed to the high concentration of dietary fibres, which are known to interact with bile salts, sometimes exerting a stabilising or structuring influence (Díaz-Piñero et al., 2024). Hypotheses to explain the interaction of dietary fibres with bile acids generally invoke two complementary mechanisms: (i) direct adsorption of bile acids by the fibre matrix through hydrophobic or physicochemical interactions (Torcello-Gómez et al., 2015; Torcello-Gómez & Foster, 2014), and (ii) the formation of a viscous fibre network that reduces bile acid release rates and limits their diffusion and reabsorption (Mackie et al., 2016; Naumann, Schweiggert-Weisz, Eglmeier, et al., 2019). However, the relative contribution of these mechanisms cannot be determined from the present data alone. Instead, the observed behaviour is likely governed by a combination of both effects, where fibre-induced increases in viscosity and matrix structuring play a dominant role in modulating bile salt mobility and spatial organisation in the intestinal lumen. Studies using cellulose derivatives (e.g., methylcellulose, hydroxypropyl cellulose) demonstrate that such fibres may bind bile salts at interfaces or in bulk, as evidenced by interfacial tension and micro-DSC experiments showing altered thermogelation behaviour in the presence of bile salts (Torcello-Gómez & Foster, 2014). Moreover, prior studies on bile salt excretion and fibre interactions demonstrated that cellulose supplementation slightly increased faecal bile salt excretion in humans (Stanley et al., 1973). The observed bile salts peak in the CAS/CEL-75 diets can also be linked to their highest proportion of polysaccharides (≈66.1%) in the digesta (cf. Table 1), which in turn led to the highest apparent viscosity (cf. Fig. 2). CMC has been reported to elevate bulk viscosity in the small intestine and slow convective–diffusive transport, thereby diminishing the diffusion and mucosal reabsorption of bile acids (Smits et al., 1998). Indeed, *in vitro* models further show that higher digesta viscosity correlates with greater bile-acid retention/partitioning by fibres, supporting a physical (mass-transfer) contribution in addition to any specific binding (Naumann, Schweiggert-Weisz, Eglmeier, et al., 2019; Zacherl et al., 2011). Thus, while the presence of dietary fibres did not significantly affect proteolysis, it seems to have a relevant impact on the types of nanostructures formed upon digestion. These observations may also be relevant in the context of lipid digestion, as bile salts play a central role in lipid emulsification, micelle formation, and solubilisation in the small intestine. Previous studies have shown that dietary fibres can modulate lipid digestion by altering bile salt availability and micellar organisation, either through direct interactions or by modifying the physicochemical environment of the intestinal lumen (Gunness & Gidley, 2010; Naumann, Schweiggert-Weisz, Eglmeier, et al., 2019; Singh et al., 2019). It is important to note that, although the structural and physicochemical changes observed here are consistent with mechanisms known to influence lipid digestion and nutrient transport, no direct measurements of lipid absorption, micellar solubilisation efficiency, or cholesterol metabolism were performed. Therefore, the functional implications proposed should be interpreted as hypotheses that warrant further targeted investigation.

Since residual starch structures were detected in the SAXS patterns from most of the ileal digests, the content of total starch present in the samples was measured, and the obtained results are shown in Table 3. As observed, the highest starch content was detected in the ileal digesta from the N-free diet (2.5%), which is reasonable since this diet contained the highest concentration of corn starch (78%). Nevertheless, the low amount of starch quantified in the ileal digesta evidence that most of it had been extensively digested, in agreement with the CLSM images. The ileal digests from the CAS and WPI diets were also among the samples with the highest starch contents (0.8% and 0.6%, respectively), which can also be linked to the relatively high amounts of corn starch in their formulations (ca. 65–67%) and is in agreement with the appearance of more defined shoulder features in the SAXS patterns. Among diets with the same protein-to-polysaccharide ratio, CAS/ALG-75 showed the highest ileal starch content, followed by CAS/CAR-75. This can be attributed to the preferential location of alginate and carrageenan on the surface of starch granules, as observed in the CLSM images (Fig. 3), and may suggest the formation of stronger interactions between these two polysaccharides and starch, thereby limiting to a certain extent the effect of amylases during the digestion process. Interestingly, the starch content in the digesta from the WPI and WPI/AG-75 diets did not differ significantly (Table 3). This supports the idea that the type and structural properties of dietary proteins and polysaccharides can influence starch digestion.

In light of the SAXS results, TEM was also used to visualise the nanostructures found in the ileal digesta. Fig. 5 presents representative TEM micrographs of the liquid fractions from the digesta. The N-free control displayed an almost featureless background with only scattered electron-dense dots. These few small particles likely correspond to minor undigested starch fragments, in agreement with the SAXS data. In contrast, the CAS digesta displayed numerous dark, irregularly shaped electron-dense regions, consistent with the presence of aggregates. Increasing agar content in the samples modified this morphology. In fact, these aggregates were no longer detected in the CAS/AG-50 and CAS/AG-75 digests. Thus, the aggregates present in CAS likely result from calcium-bridged residues that resist complete enzymatic hydrolysis, as previously reported for digested casein systems (Bayrak et al., 2021), and in line with the higher ash content of these samples (cf. Table 1). The CAS/ALG-75 digesta displayed a branched, cloud-like network of electron-dense regions, most likely due to the formation of electrostatically linked anionic alginate chains. Interestingly, the images corresponding to the CAS/CEL-75 revealed a remarkably homogeneous

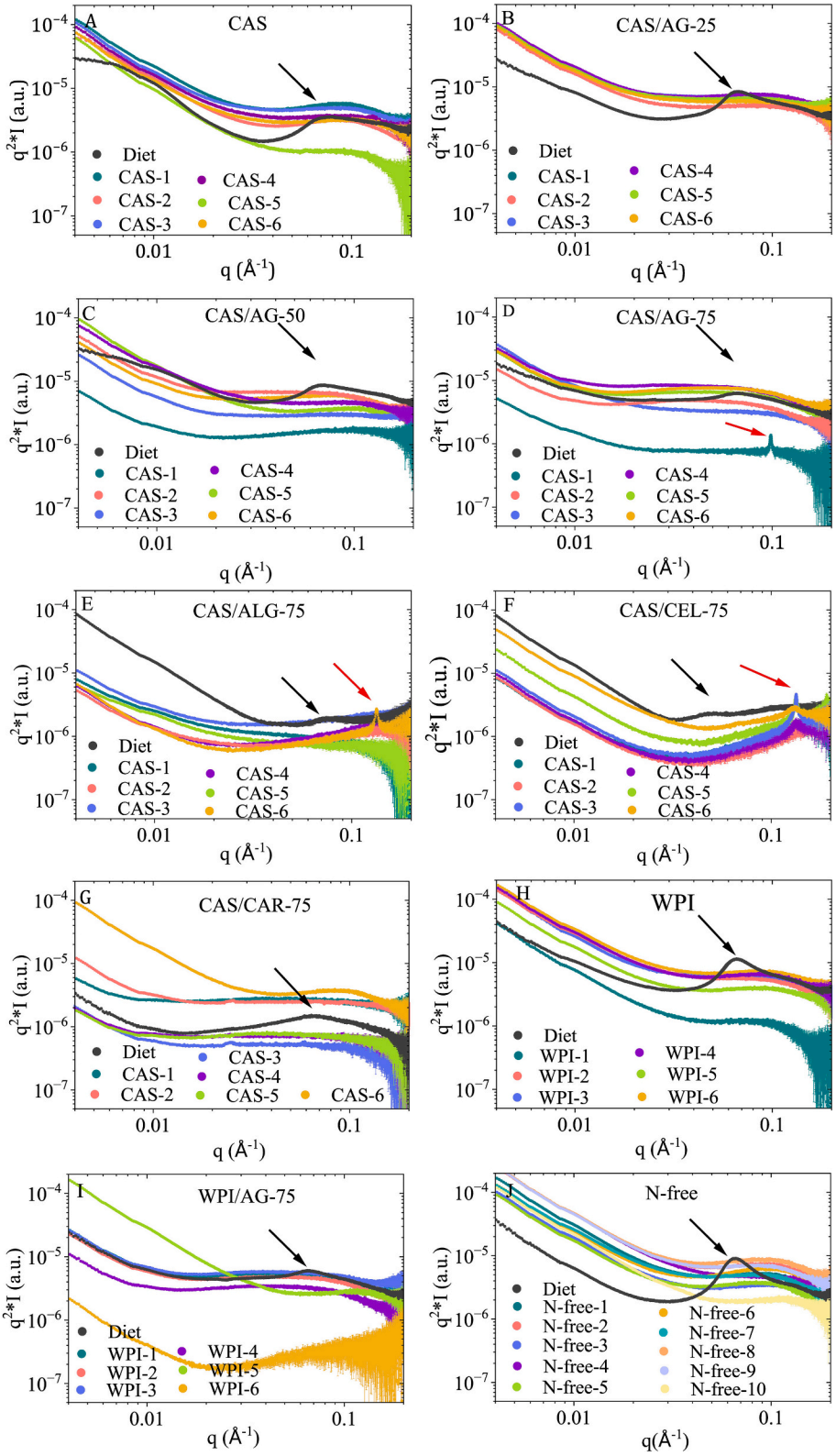

Fig. 4. SAXS Kratky plots from diets and their corresponding ileal digesta from different pigs. Each panel represents a specific formulation: (A) CAS, (B) CAS/AG-25, (C) CAS/AG-50, (D) CAS/AG-75, (E) CAS/ALG-75, (F) CAS/CEL-75, (G) CAS/CAR-75, (H) WPI (I) WPI/AG-75, and (J) N-free. Black curves correspond to the initial diet formulations, while coloured curves represent ileal digesta samples from different pigs.

dispersion of nanometric, nearly spherical aggregates with diameters ranging between 20 and 50 nm. Similar nanostructures were consistently detected in the ileal digesta from the pigs fed with this diet (Fig. S4). These aggregates could correspond to aggregated bile salt lamellae/micellar structures, in agreement with the SAXS results. Notably, WPI/AG-75 showed a greater proportion of particles than WPI, which can be linked to the protective effect of agar on specific protein domains as previously discussed.

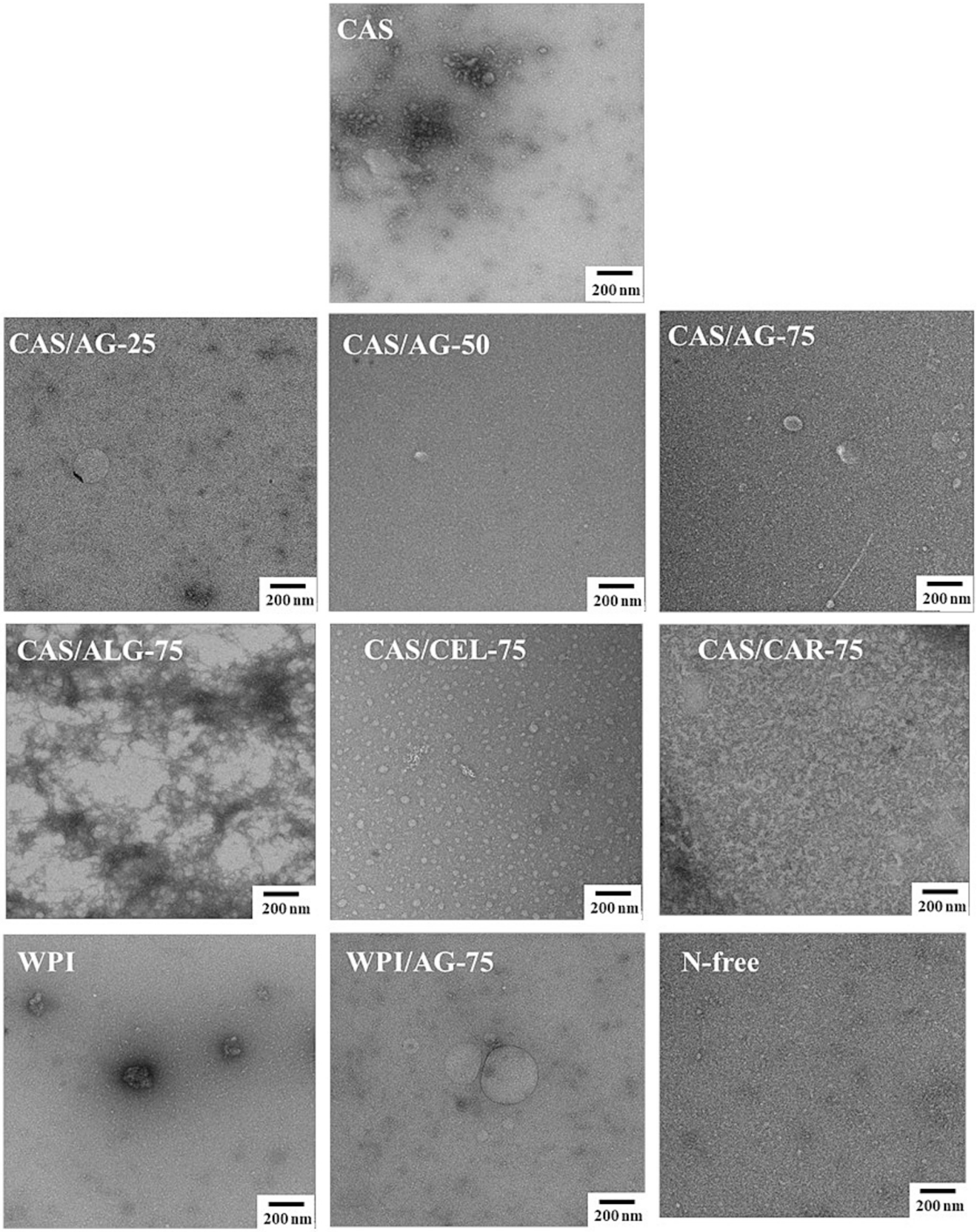

Fig. 5. Transmission Electron Microscopy (TEM) images of the liquid fractions of ileal digesta collected after *in vivo* digestion of the experimental diets.

Dynamic Light Scattering (DLS) was employed to characterise the particle size distributions in both the diets and the corresponding ileal digesta. Fig. S5 shows the size distributions for three representative ileal samples from each diet. In the initial formulations, the casein-based diets exhibited three distinct particle populations: (1) a small population below 100 nm, likely corresponding to peptide aggregates or minor colloidal species; (2) an intermediate population between 100 and 1000 nm, which can be attributed to native casein micelles (typically 150–300 nm) and casein–polysaccharide complexes; and (3) a larger population between 2000 and 10,000 nm, consistent with swollen starch granules known to hydrate during preparation (Daudt et al., 2014). The incorporation of polysaccharides markedly influenced the distribution of the first two populations, altering both their relative intensity and peak position. In particular, the CAS/CEL-75 formulation displayed a broader and more polydisperse distribution, with overlapping peaks between 100 and 1000 nm, suggesting the formation of a dense and heterogeneous matrix. This is in line with the confocal microscopy observations, which show that cellulose produces a tightly packed structure that can promote particle clustering and hinder dispersion. In contrast, the WPI-based formulations presented only two main populations: one between 30 and 100 nm, likely corresponding to whey protein aggregates, and a second one between 1000 and 5000 nm, attributed to residual starch granules. The simpler bimodal profile reflects the globular nature and higher solubility of whey proteins, which favour the formation of smaller, more uniform aggregates compared to the casein-based systems.

After ileal digestion, marked alterations were observed in the particle size distributions of all samples. The N-free digesta exhibited a bimodal distribution, with one population between 200 and 3000 nm and a larger population between 2000 and 10 μm, consistent with the presence of endogenous components such as mucins, shed epithelial vesicles, and exosome-like particles that naturally occur in the intestinal environment (Grundy et al., 2023). This observation aligns well with the CLSM images and peptidomic results, which indicated the presence of endogenous material even in the absence of dietary protein. In contrast, the ileal digesta from diets containing proteins or protein–polysaccharide blends displayed a shift toward larger particle sizes and a general broadening of the size distributions. Rather than a complete breakdown into small peptide or polysaccharide fragments, most digesta exhibited particle populations centred around 500–2000 nm, suggesting the formation of secondary aggregates during digestion. This trend agrees with the CLSM observations, where particulate material was visible across most formulations. These aggregates likely arise from electrostatic and hydrophobic interactions between non-digested polysaccharides, hydrophobic peptides, bile salts, and digestive enzymes, leading to the formation of colloidal complexes.

The ζ-potential data, shown in Fig. 6, offer valuable insights into the surface charge characteristics of the initial diets and their corresponding digesta. The initial diets exhibited strongly negative ζ-potential values, ranging from approximately −18 to −60 mV. These values indicate good colloidal stability and suggest the dominance of negatively charged surface groups, primarily provided by proteins and anionic polysaccharides present in the matrix. As clearly evidenced, the diets containing alginate and cellulose showed a higher negative net charge as compared to the N-free diet, suggesting that these two polysaccharides had a greater impact in providing negative charges. In the case of alginate, its markedly negative ζ-potential can be attributed to its high density of carboxylate groups, which remain fully ionised at physiological pH (Meskelis et al., 2024). CMC, a chemically modified cellulose derivative, also bears negatively charged carboxylate groups introduced through substitution. Unlike native cellulose, which is largely neutral, CMC exhibits a measurable negative charge due to these functional groups (Karim et al., 2014). On the other hand, the diets with CAS and WPI, with and without the addition of agar, showed less negative charges (−25 to −27 mV), which may suggest that, due to protein-polysaccharide interactions, the effect of agar in increasing the negative charges was not so evident.

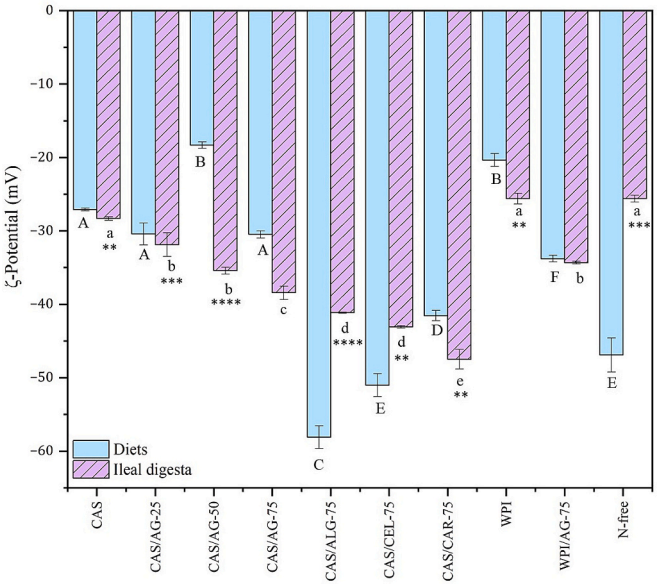

Fig. 6. Zeta potential (ζ-potential) values of the initial diets dispersed in water before digestion (blue bars) and their corresponding ileal digests (purple bars). Different letters indicate significant differences among formulations. Asterisks denote significant differences between each initial diet and its corresponding ileal digesta. (For interpretation of the references to colour in this figure legend, the reader is referred to the web version of this article.)

Following *in vivo* digestion, most of the samples displayed significant changes in ζ-potential, although the values remained highly negative, indicating sustained colloidal stability. Upon the digestion process, the starch and the proteins present in the diets were hydrolysed, and most of the released digestion products were absorbed along the intestinal epithelium, leaving only non-digestible polysaccharides, partially digested starch and a small fraction of peptides, together with endogenous components. All these components contribute to the overall surface charge of the digests, but interactions between these components will also influence the net charge. As observed, the digests from casein–agar blends showed an interesting concentration-dependent behaviour, with more negative ζ-potential as the concentration of agar in the initial diet was increased. This can be related to the non-digested agar remaining in the digests. For the same polysaccharide loading, the effect on the ζ-potential was different depending on the type of fibre. While the digests from CAS/ALG-75 and CAS/CELL-75 showed less negative values than the initial diets, the opposite effect was noted in the case of CAS/CAR-75. This behaviour may reflect the strong tendency of alginate and cellulose to interact with digestion products, particularly peptides, mucus components, and bile salts, leading to the formation of mixed colloidal aggregates with lower net charge density (Massa et al., 2022). Carrageenan is also known to form weaker complexes with peptides compared with alginate, and its limited binding may allow its negative charge to dominate the colloidal environment at the ileum (Li et al., 2023).

4. Conclusions

This study provides a comprehensive multi-scale characterisation of ileal digesta from pigs fed diets containing model milk proteins and seaweed-derived polysaccharides. Across all diets, casein and whey proteins were extensively hydrolysed, and the protein fraction of the ileal digesta was dominated by endogenous enzymes and mucosal proteins. Although fibre inclusion did not markedly impair overall protein digestion, specific protein domains appeared to be partially protected by the presence of carrageenan, alginate, and agar, especially when

combined with WPI. While *in vitro* systems suggested that fibre-induced viscosity and matrix structuring could limit proteolysis, the *in vivo* results demonstrate that protein digestion remains highly efficient across all formulations, highlighting the importance of physiological conditions in modulating these interactions.

Starch granules present in the diets were largely degraded, in agreement with CLSM observations. However, SAXS revealed small but detectable remnants of short-range starch order, particularly in starch-rich diets, suggesting the presence of a minor resistant-starch fraction.

The undigested polysaccharides exhibited distinct fibre-specific structural behaviours. Alginate-rich digesta showed evidence of network-like assemblies, whereas cellulose- and agar-containing formulations generated dense, viscous matrices that altered the physical properties of the intestinal contents. These viscosity effects were particularly evident in the CAS/CEL-75, which exhibited the highest digesta viscosity, and may be associated with modifications in bile-salt organisation and transport. In this context, our results provide clear evidence of ordered nanostructures associated with bile salts in ileal digesta, as revealed by SAXS. Furthermore, a distinct fibre-dependent effect was observed, with cellulose-containing systems showing more consistent and pronounced nanostructural organisation compared to other polysaccharides. Importantly, these findings reveal a multi-scale correlation between viscosity, microstructure, and nanostructure, linking fibre-induced physical properties to bile salt organisation in a physiological environment. At the nanoscale, TEM and DLS revealed the formation of diverse colloidal structures, including aggregates of 20–30 nm in CAS/CEL-75 digesta, as well as larger polydisperse populations (≈ 500–1500 nm) in most fibre-containing diets, likely representing digestion-induced complexes involving fibres, peptides, bile salts, and lipids.

Overall, these results show that seaweed-derived polysaccharides do not impair protein hydrolysis, but they strongly influence the structural organisation, viscosity, and bile-salt dynamics of the digesta. Together, these findings provide a mechanistic basis for designing fibre-rich functional foods that modulate digestion, intestinal transport, and lipid metabolism.

CRediT authorship contribution statement

Yubexi Correa: Writing – review & editing, Writing – original draft, Methodology, Investigation, Formal analysis, Data curation, Conceptualization. **Natalia S. Fanelli:** Writing – review & editing, Validation, Methodology, Investigation, Formal analysis, Data curation. **Juan Carlos Martínez:** Writing – review & editing, Investigation, Formal analysis, Data curation. **Cristina Jiménez-Holgado:** Investigation, Formal analysis, Data curation. **Isidra Recio:** Writing – review & editing, Validation, Resources, Methodology, Formal analysis. **Hans H. Stein:** Writing – review & editing, Validation, Supervision, Resources, Methodology, Funding acquisition, Formal analysis. **Marta Martínez-Sanz:** Writing – review & editing, Validation, Supervision, Resources, Project administration, Methodology, Investigation, Funding acquisition, Formal analysis, Conceptualization.

Declaration of competing interest

The authors declare that they have no known competing financial interests or personal relationships that could have appeared to influence the work reported in this paper.

Acknowledgements

This work was funded by the European Union (ERC, PRODIGEST, ERC-2022-COG 101086483). Views and opinions expressed are, however, those of the author(s) only and do not necessarily reflect those of the European Union or the European Research Council Executive Agency. Marta Martínez-Sanz acknowledges financial support for this research by the Fulbright U.S. Scholar Program, which is sponsored by the U.S. Department of State and the Spanish Fulbright Commission. Its contents are solely the responsibility of the author and do not necessarily represent the official views of the Fulbright Program, the Government of the United States, or the Spanish Fulbright Commission. Neither the European Union nor the granting authority can be held responsible for them. Synchrotron experiments were performed at NCD beamline at ALBA Synchrotron with the collaboration of ALBA staff (proposal 2024108915).

Appendix A. Supplementary data

Supplementary data to this article can be found online at https://doi.org/10.1016/j.foodres.2026.119614.

Data availability

Data will be made available on request.

References

Acharya, K. R., Ren, J. S., Stuart, D. I., Phillips, D. C., & Fenna, R. E. (1991). Crystal structure of human alpha-Lactalbumin at 1.7 a resolution. *Journal of Molecular Biology, 221*, 571–581.

Ávila-Arres, I. E., Rodríguez Hernández, E., Gómez Rosales, S., Reis de Souza, T. C., & Mariscal-Landín, G. (2024). Proteomic identification and quantification of basal endogenous proteins in the ileal digesta of growing pigs. *Animals, 14*, 1–15. https://doi.org/10.3390/ani14132000

Ayllón, N., Jiménez-Marín, Á., Argüello, H., Zaldívar-López, S., Villar, M., Aguilar, C., … Garrido, J. J. (2017). Comparative proteomics reveals differences in host-pathogen interaction between infectious and commensal relationship with campylobacter Jejuni. *Frontiers in Cellular and Infection Microbiology, 7*, 1–10. https://doi.org/10.3389/fcimb.2017.00145

Bayrak, M., Mata, J., Raynes, J. K., Greaves, M., White, J., Conn, C. E., … Logan, A. (2021). Investigating casein gel structure during gastric digestion using ultra-small and small-angle neutron scattering. *Journal of Colloid and Interface Science, 594*, 561–574. https://doi.org/10.1016/j.jcis.2021.03.087

Blazek, J., & Gilbert, E. P. (2011). Application of small-angle X-ray and Neutron scattering techniques to the characterisation of starch structure: A review. *Carbohydrate Polymers, 85*, 281–293. https://doi.org/10.1016/j.carbpol.2011.02.041

Boirie, Y., Dangin, M., Gachon, P., Vasson, M., Maubois, J., & Beaufrère, B. (1997). *Slow and fast dietary proteins differently modulate postprandial protein accretion. 94* pp. 14930–14935). https://doi.org/10.1073/pnas.94.26.14930

Bos, C., Metges, C. C., Gaudichon, C., Petzke, K. J., Pueyo, M. E., Morens, C., … Tomé, D. (2003). Postprandial kinetics of dietary amino acids are the Main determinant of their metabolism after soy or Milk protein ingestion in humans. *The Journal of Nutrition, 133*, 1308–1315. https://doi.org/10.1093/jn/133.5.1308

Brennan, C. S. (2005). Dietary fibre, Glycaemic response, and diabetes. *Molecular Nutrition & Food Research, 49*, 560–570. https://doi.org/10.1002/mnfr.200500025

Chater, P. I., Wilcox, M. D., Brownlee, I. A., & Pearson, J. P. (2015). Alginate as a protease inhibitor in vitro and in a model gut system; selective inhibition of pepsin but not trypsin. *Carbohydrate Polymers, 131*, 142–151. https://doi.org/10.1016/j.carbpol.2015.05.062

Chaudhary, J., Thakur, S., Sharma, M., Gupta, V. K., & Thakur, V. K. (2020). Development of biodegradable Agar-Agar/gelatin-based superabsorbent hydrogel as an efficient moisture-retaining agent. *Biomolecules, 10*, 1–13. https://doi.org/10.3390/biom10060939

Daudt, R. M., Külkamp-Guerreiro, I. C., Cladera-Olivera, F., Thys, R. C. S., & Marczak, L. D. F. (2014). Determination of properties of Pinhão starch: Analysis of its applicability as pharmaceutical excipient. *Industrial Crops and Products, 52*, 420–429. https://doi.org/10.1016/j.indcrop.2013.10.052

Díaz-Piñero, L., Correa, Y., Navas, A. C., Martínez, J. C., Recio, I., & Martínez-Sanz, M. (2026). Investigating the impact of different dietary Fibres on the gastrointestinal digestion of food proteins. *Food Hydrocolloids, 172*. https://doi.org/10.1016/j.foodhyd.2025.112182

Díaz-Piñero, L., Fontes-Candia, C., Rodríguez-Dobreva, E., Recio, I., & Martínez-Sanz, M. (2024). Influence of bile salts on the gastrointestinal digestion of Agar-casein hybrid systems and the Nanoassembly of their digestion products. *Food Research International, 197*, Article 115179. https://doi.org/10.1016/J.FOODRES.2024.115179

Dikeman, C. L., & Fahey, G. C., Jr. (2006). Viscosity as related to dietary Fiber: A review. *Critical Reviews in Food Science and Nutrition, 46*, 649–663. https://doi.org/10.1080/10408390500511862

Domozych, D. S., Ciancia, M., Fangel, J. U., Mikkelsen, M. D., Ulvskov, P., & Willats, W. G. T. (2012). The cell walls of green algae: A journey through evolution and diversity. *Frontiers in Plant Science, 3*, 1–7. https://doi.org/10.3389/fpls.2012.00082

Egger, L., Ménard, O., Baumann, C., Duerr, D., Schlegel, P., Stoll, P., … Portmann, R. (2019). Digestion of Milk proteins: Comparing static and dynamic in vitro digestion

systems with in vivo data. *Food Research International, 118*, 32–39. https://doi.org/10.1016/j.foodres.2017.12.049

Espinosa, C. D., Torres, L. J., Velayudhan, D. E., Dersjant-Li, Y., & Stein, H. H. (2022). Ileal and Total tract digestibility of energy and nutrients in pig diets supplemented with a novel consensus bacterial 6-Phytase variant. *Journal of Animal Science, 100*, 1–8. https://doi.org/10.1093/jas/skac364

Fanelli, N. S., Correa, Y., Martínez-Sanz, M., & Stein, H. H. (2026). *Protein quality of seaweeds and effects of adding seaweed polysaccharides on amino acid digestibility of high-quality proteins*. Manuscript under Revis.

Farrell, H. M., Jimenez-Flores, R., Bleck, G. T., Brown, E. M., Butler, J. E., Creamer, L. K., … Swaisgood, H. E. (2004). Nomenclature of the proteins of cows' Milk - sixth revision. *Journal of Dairy Science, 87*, 1641–1674. https://doi.org/10.3168/jds.S0022-0302(04)73319-6

Fontes-Candia, C., Díaz-Piñero, L., Carlos Martínez, J., Gómez-Mascaraque, L. G., López-Rubio, A., & Martínez-Sanz, M. (2023). Nanostructural changes in polysaccharide-casein gel-like structures upon in vitro gastrointestinal digestion. *Food Research International, 169*. https://doi.org/10.1016/j.foodres.2023.112862

Goderis, B., Dries, D. M., Nivelle, M. A., & Delcour, J. A. (2022). Reassessment of the generic features of starch gelatinization: An advanced SAXS study on maize and potato starch. *Food Hydrocolloids, 133*, Article 107941. https://doi.org/10.1016/j.foodhyd.2022.107941

Goh, K. K. T., Teo, A., Sarkar, A., & Singh, H. (2019). *Milk protein-polysaccharide interactions* (3rd ed.). Elsevier Inc (ISBN 9780128152515.).

Grundy, M. M. L., Labarre, J., Mayeur-Nickel, F., Van Milgen, J., & Renaudeau, D. (2023). An in vitro and in vivo approach to characterize Digesta from pigs fed different forms of pea flour. *Journal of Animal Science, 101*, 1–11. https://doi.org/10.1093/jas/skad037

Gunness, P., & Gidley, M. J. (2010). Mechanisms underlying the cholesterol-lowering properties of soluble dietary fibre polysaccharides. *Food & Function, 1*, 149–155. https://doi.org/10.1039/c0fo00080a

Hansen, S., Bauer, R., Lomholt, S. B., Quist, K. B., Pedersen, J. S., & Mortensen, K. (1996). Structure of casein micelles studied by small-angle neutron scattering. *European Biophysics Journal, 24*, 143–147. https://doi.org/10.1007/BF00180271

Hodgkinson, S. M., Stroebinger, N., Van Der Wielen, N., Mensink, M., Montoya, C., Hendriks, W. H., … Moughan, P. J. (2022). Comparison of true Ileal amino acid digestibility between adult humans and growing pigs. *The Journal of Nutrition, 152*, 1635–1646. https://doi.org/10.1093/jn/nxac077

Holt, C., De Kruif, C. G., Tuinier, R., & Timmins, P. A. (2003). Substructure of bovine casein micelles by small-angle X-ray and Neutron scattering. *Colloids and Surfaces A: Physicochemical and Engineering Aspects, 213*, 275–284. https://doi.org/10.1016/S0927-7757(02)00520-4

Hu, B., Chen, X., Zhai, R., Williams, P. A., Guo, J., Yang, J., … Cao, J. (2025). Effects of Milk protein concentrate decalcification on casein micelles as carriers for lutein. *Food Hydrocolloids, 167*, Article 111457. https://doi.org/10.1016/j.foodhyd.2025.111457

Jagadeesan, S., Govindaraju, I., & Mazumder, N. (2020). An insight into the ultrastructural and physiochemical characterization of potato starch: A review. *American Journal of Potato Research, 97*, 464–476. https://doi.org/10.1007/s12230-020-09798-w

Kang, X., Zhu, W., Xu, T., Sui, J., Gao, W., Liu, Z., … Abd El-Aty, A. M. (2022). Characterization of starch structures isolated from the grains of waxy, sweet, and hybrid sorghum (*Sorghum bicolor* L. Moench). *Frontiers in Nutrition, 9*. https://doi.org/10.3389/fnut.2022.1052285

Karim, M. Z., Chowdhury, Z. Z., Hamid, S. B. A., & Ali, M. E. (2014). Statistical optimization for acid hydrolysis of microcrystalline cellulose and its physiochemical characterization by using metal ion catalyst. *Materials (Basel), 7*, 6982–6999. https://doi.org/10.3390/ma7106982

Kieffer, J., & Wright, J. P. (2013). PyFAI: A Python library for high performance azimuthal integration on GPU. *Powder Diffraction, 28*, 339–350. https://doi.org/10.1017/S0885715613000924

Li, J., Yang, Z., Lin, X., Wu, S., Li, G., Li, N., , … Corke, H., et al. (2021). In-flow SAXS investigation of whey protein isolate hydrolyzed by bromelain. *Colloids and Surfaces A: Physicochemical and Engineering Aspects, 631*, 1–7. https://doi.org/10.1016/j.colsurfa.2021.127662

Li, X., Xu, Y., Kong, B., Sun, F., Liu, H., Zhang, H., … Cao, C. (2023). In vitro gastrointestinal digestibility and Peptidomic analysis of frankfurters as influenced by different forms of κ-carrageenan. *Agric. Commun., 1*, Article 100017. https://doi.org/10.1016/j.agrcom.2023.100017

Lomartire, S., & Gonçalves, A. M. M. (2022). *An Overview of Potential Seaweed-Derived Bioactive Compounds for Pharmaceutical Applications. 20*. ISBN 3512392407.

Lopez-Rubio, A., Flanagan, B. M., Shrestha, A. K., Gidley, M. J., & Gilbert, E. P. (2008). Molecular rearrangement of starch during in vitro digestion: Toward a better understanding of enzyme resistant starch formation in processed starches. *Biomacromolecules, 9*, 1951–1958. https://doi.org/10.1021/bm800213h

Mackie, A., Bajka, B., & Rigby, N. (2016). Roles for dietary fibre in the upper GI tract: The importance of viscosity. *Food Research International, 88*, 234–238. https://doi.org/10.1016/j.foodres.2015.11.011

Malila, Y., Owolabi, I. O., Chotanaphuti, T., Sakdibhornssup, N., Elliott, C. T., Visessanguan, W., … Petchkongkaew, A. (2024). Current challenges of alternative proteins as future foods. *npj Science of Food, 8*. https://doi.org/10.1038/s41538-024-00291-w

Mamone, G., & Picariello, G. (2023). Optimized extraction and large-scale proteomics of pig jejunum brush border membranes for use in in vitro digestion models. *Food Research International, 164*, Article 112326. https://doi.org/10.1016/j.foodres.2022.112326

Massa, M., Compari, C., & Fisicaro, E. (2022). On the mechanism of the cholesterol lowering ability of soluble dietary fibers: Interaction of some bile salts with pectin, alginate, and chitosan studied by isothermal titration calorimetry. *Frontiers in Nutrition, 9*, 1–13. https://doi.org/10.3389/fnut.2022.968847

Megazyme, L. (2009). Total Starch Assay Procedure K-TSTA. Total starch assay kit-for Determ. *Total Starch| Megazyme*.

Meskelis, L., Agondi, F. R., Duarte, L. G. R., de Carvalho, M. D., Sato, A. C. K., & Picone, C. S. F. (2024). New approaches for modulation of alginate-chitosan delivery properties. *Food Research International, 175*, Article 113737. https://doi.org/10.1016/j.foodres.2023.113737

Müller-Buschbaum, P., Gebhardt, R., Roth, S. V., Metwalli, Z. E., & Doster, W. (2007). Effect of calcium concentration on the structure of casein micelles in thin films. *Biophysical Journal, 93*, 960–968. https://doi.org/10.1529/biophysj.107.106385

Naumann, S., Schweiggert-Weisz, U., Eglmeier, J., Haller, D., & Eisner, P. (2019). In vitro interactions of dietary fibre enriched food ingredients with primary and secondary bile acids. *Nutrients, 11*, 1–18. https://doi.org/10.3390/nu11061424

Naumann, S., Schweiggert-Weisz, U., Haller, D., & Eisner, P. (2019). Retention of primary bile acids by Lupin Cell Wall polysaccharides under in vitro digestion conditions. *Nutrients, 11*, 1–19. https://doi.org/10.3390/nu11092117

Paleekui, P., Rattanamato, B., Kanha, N., Rakariyatham, K., Klangpetch, W., Osiriphun, S., & Laokuldilok, T. (2025). Texture-modified soy protein gels using transglutaminase and agar for elderly dysphagia management. *Gels, 11*, 1–18. https://doi.org/10.3390/gels11040303

Pignon, F., Belina, G., Narayanan, T., Paubel, X., Magnin, A., & Gésan-Guiziou, G. (2004). Structure and rheological behavior of casein micelle suspensions during ultrafiltration process. *The Journal of Chemical Physics, 121*, 8138–8146. https://doi.org/10.1063/1.1800931

Rowan, A. M., Moughan, P. J., Wilson, M. N., Maher, K., & Tasman-Jones, C. (1994). Comparison of the Ileal and Faecal digestibility of dietary amino acids in adult humans and evaluation of the pig as a model animal for digestion studies in man. *The British Journal of Nutrition, 71*, 29–42. https://doi.org/10.1079/bjn19940108

Sadiq, U., Gill, H., & Chandrapala, J. (2021). Casein micelles as an emerging delivery system for bioactive food components. *Foods, 10*. https://doi.org/10.3390/foods10081965

Salehi, B., Sharifi-rad, J., Seca, A. M. L., & Pinto, D. C. G. A. (2019). Current trends on seaweeds : Looking at chemical. *Molecules, 24*, 4182.

Dr. Latimer, George W, Jr. (ed.), Official Methods of Analysis of AOAC INTERNATIONAL, 22nd Edition (New York, 2023; online edn, AOAC Publications, 4 Jan. 2023), https://doi.org/10.1093/9780197610145.001.0001, accessed 2 June 2026.

Singh, H.; Ye, A.; Ferrua, M.J. Aspects of food structures in the digestive tract. Current Opinion in Food Science *3*, 85–93, doi:https://doi.org/10.1016/j.cofs.2015.06.007.

Singh, J., Metrani, R., Shivanagoudra, S. R., Jayaprakasha, G. K., & Patil, B. S. (2019). Review on bile acids: Effects of the gut microbiome, interactions with dietary Fiber, and alterations in the bioaccessibility of bioactive compounds. *Journal of Agricultural and Food Chemistry, 67*, 9124–9138. https://doi.org/10.1021/acs.jafc.8b07306

Smits, C. H., Veldman, A., Verkade, H. J., & Beynen, A. C. (1998). The inhibitory effect of Carboxymethylcellulose with high viscosity on lipid absorption in broiler chickens coincides with reduced bile salt concentration and raised microbial numbers in the small intestine. *Poultry Science, 77*, 1534–1539. https://doi.org/10.1093/ps/77.10.1534

Stanley, M. M., Paul, D., Gacke, D., & Murphy, J. (1973). Effects of cholestyramine, Metamucil, and cellulose on fecal bile salt excretion in man. *Gastroenterology, 65*, 889–894. https://doi.org/10.1016/s0016-5085(19)32980-4

Stein, H. H. (2024). The pig is an excellent model to determine amino acid digestibility of human foods and to generate data needed to meet human amino acid requirements. *Frontiers in Nutrition, 11*, 1–7. https://doi.org/10.3389/fnut.2024.1434430

Stein, H. H., Shipley, C. F., & Easter, R. A. (1998). Technical note: A technique for inserting a T-cannula into the distal ileum of pregnant sows. *Journal of Animal Science, 76*, 1433–1436. https://doi.org/10.2527/1998.7651433x

Štreimikytė, P., Keršienė, M., Eisinaitė, V., Jasutienė, I., Lesauskaitė, V., Damulevičienė, G., … Leskauskaitė, D. (2020). Formulating protein-based beverages for the dysphagia diets of the elderly: Viscosity, protein quality, in vitro digestion, and consumers acceptability. *Journal of the Science of Food and Agriculture, 100*, 3895–3901. https://doi.org/10.1002/jsfa.10431

Torcello-Gómez, A., Fernández Fraguas, C., Ridout, M. J., Woodward, N. C., Wilde, P. J., & Foster, T. J. (2015). Effect of substituent pattern and molecular weight of cellulose ethers on interactions with different bile salts. *Food & Function, 6*, 730–739. https://doi.org/10.1039/c5fo00099h

Torcello-Gómez, A., & Foster, T. J. (2014). Interactions between cellulose ethers and a bile salt in the control of lipid digestion of lipid-based systems. *Carbohydrate Polymers, 113*, 53–61. https://doi.org/10.1016/j.carbpol.2014.06.070

Van De Velde, F., Van Riel, J., & Tromp, R. H. (2002). Visualisation of starch granule morphologies using confocal scanning laser microscopy (CSLM). *Journal of the Science of Food and Agriculture, 82*, 1528–1536. https://doi.org/10.1002/jsfa.1165

Vasconcelos, M. M. M., Marson, G. V., Rioux, L. E., Tamigneaux, E., Turgeon, S. L., & Beaulieu, L. (2023). In vitro bioaccessibility of proteins and bioactive compounds of wild and cultivated seaweeds from the Gulf of Saint Lawrence. *Marine Drugs, 21*. https://doi.org/10.3390/md21020102

Wu, P., Dhital, S., Williams, B. A., Chen, X. D., & Gidley, M. J. (2016). Rheological and microstructural properties of porcine gastric Digesta and diets containing pectin or mango powder. *Carbohydrate Polymers, 148*, 216–226. https://doi.org/10.1016/j.carbpol.2016.04.037

Xie, C., Lee, Z. J., Ye, S., Barrow, C. J., Dunshea, F. R., & Suleria, H. A. R. (2024). A review on seaweeds and seaweed-derived polysaccharides: Nutrition, chemistry, bioactivities, and applications. *Food Review International, 40*, 1312–1347. https://doi.org/10.1080/87559129.2023.2212055

Ye, S., Xie, C., Agar, O. T., Barrow, C. J., Frank, R., & Suleria, H. A. R. (2023). Alginates from Brown seaweeds as a promising natural source : A review of its properties and health benefits. *Food Review International, 00*, 1–29. https://doi.org/10.1080/87559129.2023.2279583

You, L., Gong, Y., Li, L., Hu, X., Brennan, C., & Kulikouskaya, V. (2020). Beneficial effects of three Brown seaweed polysaccharides on gut microbiota and their structural characteristics: An overview. *International Journal of Food Science and Technology, 55*, 1199–1206. https://doi.org/10.1111/ijfs.14408

Zacherl, C., Eisner, P., & Engel, K. H. (2011). In vitro model to correlate viscosity and bile acid-binding capacity of digested water-soluble and insoluble dietary Fibres. *Food Chemistry, 126*, 423–428. https://doi.org/10.1016/j.foodchem.2010.10.113